MATERIALS SCIENCE

Enhanced medium-range order in vapor-deposited germania glasses at elevated temperatures

Le Yang[1]*, Gabriele Vajente[2], Mariana Fazio[3], Alena Ananyeva[2], GariLynn Billingsley[2], Ashot Markosyan[4], Riccardo Bassiri[4], Kiran Prasai[4], Martin M. Fejer[4], Martin Chicoine[5], François Schiettekatte[5], Carmen S. Menoni[1,3]*

Glasses are nonequilibrium solids with properties highly dependent on their method of preparation. In vapor-deposited molecular glasses, structural organization could be readily tuned with deposition rate and substrate temperature. Here, we show that the atomic arrangement of strong network-forming GeO_2 glass is modified at medium range (<2 nm) through vapor deposition at elevated temperatures. Raman spectral signatures distinctively show that the population of six-membered GeO_4 rings increases at elevated substrate temperatures. Deposition near the glass transition temperature is more efficient than postgrowth annealing in modifying atomic structure at medium range. The enhanced medium-range organization correlates with reduction of the room temperature internal friction. Identifying the microscopic origin of room temperature internal friction in amorphous oxides is paramount to design the next-generation interference coatings for mirrors of the end test masses of gravitational wave interferometers, in which the room temperature internal friction is a main source of noise limiting their sensitivity.

INTRODUCTION

Glasses are nonequilibrium, noncrystalline materials that retain in their structure at short- and medium-range (<2 nm) information about the history of preparation (*1*, *2*). For melt-quenched glasses, a slow cooling rate toward the glass transition temperature (T_g) allows for an adequate configurational sampling that drives the system to lower energy states in the potential energy landscape (PEL). Physical vapor deposition is an efficient means of rapid cooling to produce glassy materials. Altering the deposition conditions, such as substrate temperature (T_{sub}) and deposition rate, makes it possible to manipulate the atomic ordering that, in turn, shapes the properties of the vapor-deposited glasses (*3*–*6*). For example, in vapor-deposited thin films of itraconazole, a glass-forming smectic liquid crystal, the orientation of the molecule's long axis tends to align with the surface normal when the deposition rate is around 0.2 Å/s, whereas nearly isotropic orientation is preferred when the deposition rate is three orders of magnitude higher (*7*). In a similar fashion, T_{sub} plays a role in affecting the molecular packing in thin-film organic glasses. Depositing *N*,*N*′-bis(3-methylphenyl)-*N*,*N*′-diphenylbenzidine at around 0.8 T_g produces glasses with a strong horizontal orientation, while at 0.95 T_g, weak vertical orientation is observed (*3*, *8*). In silico vapor deposition of glasses predicts that when depositing at the Kauzmann temperature, where the configurational entropy vanishes, it would be possible to achieve a uniform structural configuration characteristic of ultrastable glassy materials (*9*). It remains to be answered experimentally whether the atomic arrangement of strong network-forming glasses, such as amorphous SiO_2 (a-SiO_2) and GeO_2 (a-GeO_2), could be modified by altering the T_{sub} because the restructuring of strong covalent bonds is involved.

A question that follows is whether elevated temperature deposition of a-GeO_2 would result in atomic rearrangements that alter the distribution of two-level systems (TLSs) in glassy materials. TLSs in the PEL model are used to describe the acoustic and thermal properties of amorphous solids at low temperatures (*10*). They are represented by asymmetric double-well potentials in some configuration coordinate. Transitions between the wells, which are thermally activated at temperatures above ~5 K, and quantum tunneling dominated at lower temperatures, are associated with the rearrangement of a small group of atoms at temperatures well below T_g (*11*). Recent insights into the properties of vapor-deposited glasses show that TLSs could possibly be drastically reduced at selected deposition conditions (*2*). In indomethacin thin-film glasses grown at 0.85 T_g, remarkable suppression of TLSs was found because of the particular molecular arrangement influenced by the deposition conditions (*12*). For network-forming glasses such as a-Si, the density of TLSs has been shown to be reduced by at least one order of magnitude when T_{sub} increased from 473 to 673 K (*13*, *14*). This behavior has been ascribed to a more ordered amorphous network achieved with elevated temperature deposition. Motivated by these results, the gravitational wave community has explored the possibility to lower the density of TLSs through elevated temperature deposition of a-Ta_2O_5 as a way to reduce room temperature internal friction in the coatings of the end test mass mirrors (*15*, *16*). Internal friction in amorphous materials is generally framed in terms of energy coupling from an elastic field into TLSs. The coupling causes excitations visualized as transitions between the two wells in a TLS. The relaxation of these excitations through various mechanisms characterizes the system's internal friction (*17*, *18*). Room temperature internal friction, in accord with the fluctuation-dissipation theorem (*19*), leads to thermally driven fluctuations in the amorphous coatings that limit the sensitivity of gravitational wave detectors (*20*–*22*). Recent work in a-Si thin films showed that room temperature internal friction reduced from around 2×10^{-4} to 0.5×10^{-4} when T_{sub} increased from

[1]Department of Chemistry, Colorado State University, Fort Collins, CO 80523, USA. [2]LIGO Laboratory, California Institute of Technology, Pasadena, CA 91125, USA. [3]Department of Electrical and Computer Engineering, Colorado State University, Fort Collins, CO 80523, USA. [4]Edward L. Ginzton Laboratory, Stanford University, Stanford, CA 94305, USA. [5]Département de Physique, Université de Montréal, Québec H3C 3J7, Canada.
*Corresponding author. Email: yangle@colostate.edu (L.Y.); carmen.menoni@colostate.edu (C.S.M.)

293 to 673 K (~ 0.80 T_g) (*23*, *24*). Nevertheless, a correlation between structural organization and room temperature internal friction for strong network-forming glasses deposited at elevated T_{sub} is still lacking.

Here, we describe the modifications in the atomic configuration at medium range of a-GeO_2 thin films vapor-deposited at elevated T_{sub}s. The lower T_g of GeO_2, around 788 K (*25*), in comparison with T_g around 1475 K for SiO_2 (*26*), makes the deposition at T_{sub} near T_g accessible. The signatures of structural ordering, obtained from Raman spectroscopy, distinctively show that the arrangement of GeO_4 tetrahedra into six-membered rings increases when depositing at elevated T_{sub}s. It is also demonstrated that the deposition near T_g is more efficient than postgrowth annealing in modifying the atomic structure at medium range. These structural modifications correlate with the room temperature internal friction of a-GeO_2 thin films, which decreases by as much as 44% when the film is deposited at 0.83 T_g. In combination, the results demonstrate a strong correlation between medium-range order and room temperature internal friction as predicted by theory.

RESULTS

The physical vapor deposition of amorphous oxides is characterized by hit-and-stick processes in which the atomic relaxation and formation of a more stable structure are constrained when T_{sub} is low. Elevated T_{sub} and postdeposition annealing alter the organizational state of the deposited glasses by enabling the system to explore nearby lower minima in the energy landscape through atomic rearrangements. For a-GeO_2 that has strong directional covalent bonding, the most dominant structural order is at the medium range, which can be defined in terms of the connection of the GeO_4 tetrahedra (*27*–*29*). The (Ge-O-Ge) connection chain has a ring shape with a size that is determined by the number of Ge atoms within the closed path. Rings of various sizes ranging from 3 to 10 with a maximum distribution of around six-membered rings are predicted by models of a-GeO_2 (*30*). This structural information can be obtained from x-ray and neutron diffraction in combination with modeling (*30*, *31*) or alternatively from Raman spectroscopy that is sensitive to local vibrations at the medium range in glasses.

The Raman spectra of a-GeO_2 thin films, shown in Fig. 1, are characterized by strong peaks at around 430 and 510 cm^{-1}. The former corresponds to the symmetric stretching of bridging oxygen in six-membered rings (A_6) (*32*). The latter corresponds to the oxygen-breathing mode associated with three-membered rings (A_3) (*33*, *34*). Two Raman bands at 560 and 595 cm^{-1} assigned to the transverse optical and longitudinal optical asymmetric stretching of bridging oxygen, respectively (fig. S1), overlap with A_3. This overlap introduces substantial uncertainty in the fitting of the A_3 peak at 510 cm^{-1}. The integrated A_6 area was normalized to the total integrated area of the Raman spectrum between 200 and 700 cm^{-1} to evaluate the change in the population of six-membered rings. Figure 1 qualitatively contrasts the difference in the ring distribution of a-GeO_2 samples deposited at T_{sub} = room temperature and T_{sub} = 0.83 T_g, which indicates that high-temperature deposition favors a larger fraction of six-membered rings, i.e., a more ordered structure, as described below.

We focus first on the evolution of the ring distribution in a-GeO_2 deposited at T_{sub} = room temperature as the system approaches lower energy states with postdeposition annealing, visualized as changes in normalized A_6 in Fig. 2. A_6 does not significantly vary after the first annealing step at an annealing temperature (T_{an}) = 573 K. A_6 shows a pronounced increase of 29% to 0.63 ± 0.04 after annealing at T_{an} = 623 K. Annealing to higher temperature continues to relax the atomic structure, leading to an increase of A_6 to 0.72 ± 0.03. Overall, the trend indicates that the population of large six-membered rings increases. The breakup of small (three- or four-membered) rings, qualitatively identified by a reduction in the A_3 peak intensity, could be attributed to heavily strained intertetrahedral bridging bonds (*35*, *36*). The increase in the population of six-membered rings indicates that an increased medium-range order is achieved in a-GeO_2 thin films upon annealing.

Deposition at elevated T_{sub} brings more notable changes to the ring distribution in a-GeO_2, as shown in Fig. 2. A_6 is 0.58 ± 0.03 for the sample deposited at T_{sub} = 0.83 T_g and 0.47 ± 0.02 for the sample deposited at T_{sub} = room temperature. The larger fraction of six-membered rings confirms the formation of a more ordered atomic structure at elevated T_{sub}. Moreover, the results show that the T_{an} required to achieve a high medium-range order before crystallization, defined by A_6 ~ 0.71, is lower at T_{an} = 573 K, when a-GeO_2 is deposited at T_{sub} = 0.83 T_g, in comparison to T_{an} = 673 K for the a-GeO_2 deposited at T_{sub} = room temperature. Further

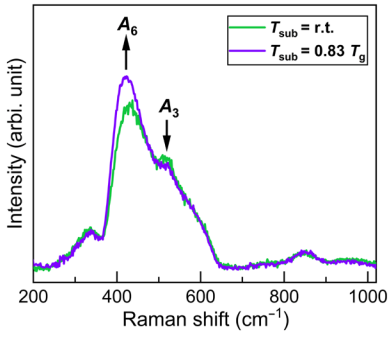

Fig. 1. Raman scattering spectra of a-GeO_2 thin films deposited at different temperatures. T_{sub} = room temperature (r.t.; green) and T_{sub} = 0.83 T_g (purple). The A_6 peak at around 430 cm^{-1} corresponds to the symmetric stretching of bridging oxygen in six-membered rings. The A_3 peak at around 510 cm^{-1} corresponds to the breathing motion of bridging oxygen in three-membered rings. The peak at 337 cm^{-1} is assigned to the Ge "deformation" motion within the network (*33*, *34*).

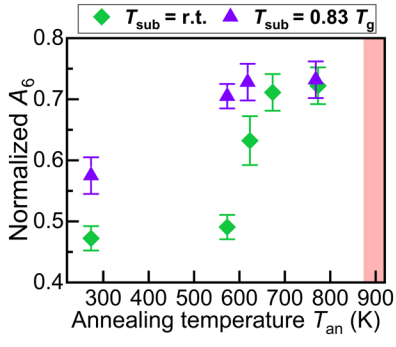

Fig. 2. Structural relaxation in a-GeO_2 thin films identified by changes in normalized A_6 versus T_{an}. Samples deposited at T_{sub} = room temperature and T_{sub} = 0.83 T_g are represented by green rhomboids and purple triangles, respectively. The temperature on each annealing step was held for 10 hours. The red shaded region in the figure indicates the start of crystallization at around 873 K for all samples.

annealing of the sample deposited at T_{sub} = 0.83 T_g to T_{an} = 773 K resulted in increased normalized A_6 ~ 0.72. All samples remained amorphous after annealing at T_{an} = 773 K for 10 hours (figs. S2 and S3). During room temperature deposition, incident sputtered particles rapidly lose their energy to the substrate before exploring the entire configuration space (*37*), whereas elevated T_{sub} promotes a larger sampling that leads to a higher degree of organization. It is through elevated T_{sub} that vapor-deposited glasses are able to achieve a more ordered structural organization (*9*, *38*, *39*).

The structural rearrangements at medium range play a role in lowering the potential energy of the glass system and are strongly dependent on the T_{sub}, as recently shown in molecular dynamic simulations of vapor-deposited a-SiO_2 films (*39*). In comparison to a-SiO_2 films deposited at T_{sub} well below T_g, the films with lower potential energy prepared at the optimal T_{sub} near T_g have a higher fraction and a narrower distribution of rings centered at six-membered rings, suggesting a greater structural uniformity.

The changes in the medium-range order of a-GeO_2 and their impact in modifying thermally activated TLSs are assessed from the room temperature internal friction Q^{-1} of thin films deposited at different T_{sub} and postdeposition annealed. Q^{-1} will refer to internal friction at room temperature unless otherwise noted. Previous modeling and experimental results of amorphous oxides, such as a-Ta_2O_5, have suggested that an increased medium-range order correlates with the reduction in Q^{-1} (*40*, *41*) at room temperature. The evolution of Q^{-1} for a-GeO_2 deposited at T_{sub} = room temperature with annealing is shown in Fig. 3A. The as-prepared a-GeO_2 thin film has a Q^{-1} of (2.98 ± 0.27) × 10^{-4}, which reduces to (2.56 ± 0.52) × 10^{-4} after the first annealing step at T_{an} = 573 K. A significant decrease by 49% is obtained after the T_{an} = 623 K annealing step. Notably, the T_{an} after which Q^{-1} undergoes a sharp decrease, coincides with the turning point in the increase of normalized A_6 in Fig. 2. Beyond T_{an} = 673 K, Q^{-1} plateaus at a value of (1.00 ± 0.13) × 10^{-4}.

Comparison of Q^{-1} for as-prepared a-GeO_2 deposited at T_{sub} = room temperature, T_{sub} = 0.60 T_g, and T_{sub} = 0.83 T_g shows a steady decrease with an increase in T_{sub}. The a-GeO_2 sample deposited at T_{sub} = 0.83 T_g has the lowest Q^{-1} = (1.66 ± 0.14) × 10^{-4}, which is 44% less than Q^{-1} of the sample deposited at room temperature. Figure 3 shows a reduction in Q^{-1} with T_{an} for all samples, although the rate at which Q^{-1} reaches its minimum value is different for each one.

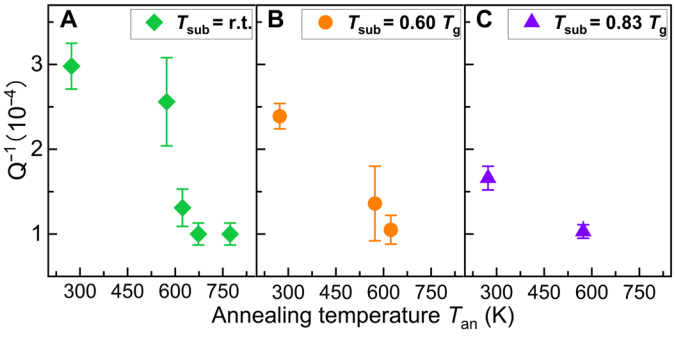

Fig. 3. Room temperature internal friction Q^{-1} of a-GeO_2 thin films deposited at different temperatures. (**A**) T_{sub} = room temperature (green), (**B**) T_{sub} = 0.60 T_g (orange), and (**C**) T_{sub} = 0.83 T_g (purple). The T_{an} to reach the lowest room temperature internal friction is T_{an} = 673 K, T_{an} = 623 K, and T_{an} = 573 K for samples deposited at T_{sub} = room temperature (green), T_{sub} = 0.60 T_g (orange), and T_{sub} = 0.83 T_g (purple), respectively.

The a-GeO_2 thin film prepared at T_{sub} = 0.60 T_g reaches Q^{-1} = 1.00 × 10^{-4} after annealing at T_{an} = 623 K, yet the one prepared at T_{sub} = 0.83 T_g achieves this Q^{-1} after annealing at T_{an} = 573 K. Annealing beyond T_{an} = 623 K does not decrease Q^{-1} below 1.00 × 10^{-4} for the high-temperature deposited samples. It is also worth noting that the a-GeO_2 thin film deposited at T_{sub} = 0.60 T_g (473 K) without thermal treatment has Q^{-1} = (2.39 ± 0.15) × 10^{-4}, which is comparable to Q^{-1} = (2.56 ± 0.52) × 10^{-4} for the sample deposited at room temperature and annealed at T_{an} = 573 K for 10 hours. Considering that the same level Q^{-1} is obtained at a lower T_{an} during a significantly shorter deposition time of around 1 hour compared to annealing for 10 hours, it indicates a higher efficiency of elevated temperature deposition over annealing for reducing Q^{-1} of a-GeO_2 thin films.

The inverse relationship of Q^{-1} with normalized A_6 in Fig. 4 demonstrates a strong and direct correlation between lowering Q^{-1} and increasing medium-range order characterized by a larger fraction of six-membered rings in a-GeO_2. Such observation echoes what has been found for vapor-deposited a-SiO_2 (*42*), where a steady decrease in the population of three-membered rings is linked to the reduction in Q^{-1} during extended annealing. Similar behavior has also been observed in (*43*), in which analyses of grazing-incidence pair distribution functions of ZrO_2-doped Ta_2O_5 reveal a systematic change in the medium-range order with T_{an}. Modeling shows that the atomic rearrangements that occur at medium range involve a decrease in the population of edge- and face-sharing polyhedra and an increase in corner-sharing ones, which agree with an expansion in the polyhedral ring connection. These modifications correlate with a steady decrease in Q^{-1} at room temperature. Further evidence directly linking the structural changes with TLSs for ZrO_2-doped Ta_2O_5 is obtained from (*44*). In this work, the energy landscape of ZrO_2-doped Ta_2O_5 was explored by searching for TLSs using molecular dynamic simulations. It is found that the TLSs can be sorted into two types depending on whether the cation-oxygen bond within the polyhedron breaks, namely, cage-breaking and non–cage-breaking transitions. The simulations show that a significant number of TLSs from cage-breaking events are responsible for room temperature Q^{-1} in the amorphous oxide. Elimination of these transitions by expanding the polyhedral connections, i.e., increasing the ring size, would thus result in lower Q^{-1}. In combination, these theories provide a consistent interpretation of the correlation between Q^{-1} and medium-range order observed in a-GeO_2 thin films.

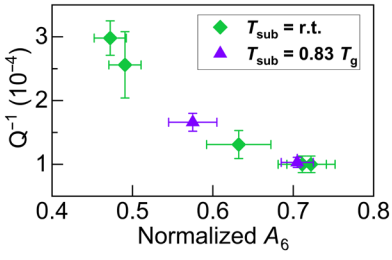

Fig. 4. Room temperature internal friction Q^{-1} as a function of normalized A_6 for a-GeO_2 thin films deposited at different T_{sub} and subsequently annealed. Samples deposited at T_{sub} = room temperature and T_{sub} = 0.83 T_g are represented by green and purple marks, respectively.

DISCUSSION

The results conclusively show that the atomic organization of strong network-forming a-GeO_2 can be modified with elevated temperature deposition, similar to the behavior observed in organic glasses (*3*–*8*). The changes in the atomic arrangement are characterized by an increase in the fraction of six-membered rings. This structural reorganization corresponds to an increase in medium-range order, which is more notable when a-GeO_2 is deposited at T_{sub} = 0.83 T_g compared to films deposited at T_{sub} = room temperature and subsequently annealed.

Furthermore, the results establish a strong correlation between medium-range order and room temperature internal friction in a-GeO_2. The more ordered atomic arrangement leads to a reduction in room temperature internal friction of as much as 44% when the film is deposited at T_{sub} = 0.83 T_g compared to T_{sub} = room temperature. Under optimum deposition and annealing conditions, the room temperature internal friction of a-GeO_2 reaches a value of $Q^{-1} = 1.00 \times 10^{-4}$, which is among the lowest in amorphous oxides and comparable to vapor-deposited a-SiO_2 (*42*). These findings are relevant for identifying suitable amorphous oxide candidates for mirror coatings of the end test masses of gravitational wave interferometers, in which the coating's room temperature internal friction is the main source of noise limiting their sensitivity.

MATERIALS AND METHODS

a-GeO_2 thin films were deposited with a 4Wave Laboratory Alloy and Nanolayer System physical vapor deposition system (*45*, *46*). A gridless ion source was used to generate low-energy Ar ions that were accelerated toward a high-purity Ge target negatively biased at 800 V. This created a sputter plume that deposited onto the substrate. Oxidation was achieved by flowing 6 standard cubic centimeters per minute of oxygen near the substrate surface. For high-temperature deposition, a heating lamp was positioned under the rotating substrate stage. The stage temperature was increased to the set point 10 min before deposition for equilibration purposes and maintained through the process. The rate for room temperature and high-temperature deposition was kept at 1.1 and 1.2 Å/s, respectively. The use of approximately the same deposition rate ruled out the influence of this parameter in atomic reorganization. Thermal annealing of each sample after deposition was carried out under ambient conditions by ramping up the temperature by 100 K/hour to T_{an}, holding at T_{an} for 10 hours, and ramping down at 100 K/hour to room temperature.

Raman scattering was performed with a HORIBA LabRAM HR Evolution Spectrometer. A frequency-doubled Nd:YAG laser of 532-nm wavelength and 10-mW average power was used for excitation. The laser beam was focused onto the sample's surface using a ×100 objective. Three spectra of 60-s acquisition time were collected for each sample and averaged to improve the signal to noise. Deconvolution of the peaks in the Raman spectrum was carried out by fitting the peaks with Gaussian line shapes. The Raman spectrum contains a peak at 337 cm^{-1} that corresponds to the Ge motion within the network; A_6 that corresponds to six-membered rings at 430 cm^{-1} (table S1); and the broad feature composed of the dominant A_3 peak at 510 cm^{-1} associated with three-membered rings and peaks at 560 and 595 cm^{-1} associated with the Ge-O-Ge bending modes. In the fitting, the full width at half maximum of A_3 was constrained to 75 cm^{-1} (*47*). The overlap of A_3 with the peaks at 560 and 595 cm^{-1} produces a high uncertainty in the calculation of the A_3 area. It is for this reason that we use the area of A_6 normalized to the area of the spectrum from 200 to 700 cm^{-1} to represent changes in the population of six-membered rings.

Room temperature internal friction (Q^{-1}) of the a-GeO_2 thin films was measured with a ring down system (*48*, *49*). The ~500-nm-thick a-GeO_2 samples for this purpose were deposited on high-quality fused silica disk of 75-mm diameter and 1-mm thickness. A gentle nodal suspension method was used to support the sample inside a vacuum chamber held at a pressure below 10^{-6} Torr. After exciting the resonant mode, the oscillation amplitude at each frequency f_i was tracked to obtain the decay time τ_i. The room temperature internal friction Q_i^{-1} for each mode was then computed through the following relation

$$Q_i^{-1} = 1/(\pi f_i \tau_i)$$

At each frequency, eight measurements were performed to obtain an averaged Q_i^{-1}. A mean value of Q^{-1} for each sample was then obtained by averaging the Q_i^{-1} over a frequency range of 1 to 20 kHz.

Rutherford backscattering spectrometry (RBS) analyses were performed using He^+ ions at 2.035 MeV with a 1.7-MV Tandetron accelerator. Spectra were acquired with samples on Si substrates tilted at 7° to minimize channeling. The scattered ions were collected at an angle of 10° from the beam. The experimental spectra were simulated using the SIMNRA software (*50*) to extract the composition and areal atomic density of the deposited layers. All samples were stoichiometric after annealing at 773 K (table S2).

SUPPLEMENTARY MATERIALS

Supplementary material for this article is available at https://science.org/doi/10.1126/sciadv.abh1117

REFERENCES AND NOTES

1. P. G. Debenedetti, F. H. Stillinger, Supercooled liquids and the glass transition. *Nature* **410**, 259–267 (2001).
2. M. D. Ediger, Perspective: Highly stable vapor-deposited glasses. *J. Chem. Phys.* **147**, 210901 (2017).
3. S. S. Dalal, D. M. Walters, I. Lyubimov, J. J. de Pablo, M. D. Ediger, Tunable molecular orientation and elevated thermal stability of vapor-deposited organic semiconductors. *Proc. Natl. Acad. Sci. U.S.A.* **112**, 4227–4232 (2015).
4. S. S. Dalal, M. D. Ediger, Molecular orientation in stable glasses of indomethacin. *J. Phys. Chem. Lett.* **3**, 1229–1233 (2012).
5. K. Bagchi, M. D. Ediger, Controlling structure and properties of vapor-deposited glasses of organic semiconductors: Recent advances and challenges. *J. Phys. Chem. Lett.* **11**, 6935–6945 (2020).
6. S. F. Swallen, K. L. Kearns, M. K. Mapes, Y. S. Kim, R. J. McMahon, M. D. Ediger, T. Wu, L. Yu, S. Satija, Organic glasses with exceptional thermodynamic and kinetic stability. *Science* **315**, 353–356 (2007).
7. C. Bishop, A. Gujral, M. F. Toney, L. Yu, M. D. Ediger, Vapor-deposited glass structure determined by deposition rate-substrate temperature superposition principle. *J. Phys. Chem. Lett.* **10**, 3536–3542 (2019).
8. A. Gujral, K. A. O'Hara, M. F. Toney, M. L. Chabinyc, M. D. Ediger, Structural characterization of vapor-deposited glasses of an organic hole transport material with X-ray scattering. *Chem. Mater.* **27**, 3341–3348 (2015).
9. S. Singh, M. D. Ediger, J. J. de Pablo, Ultrastable glasses from in silico vapour deposition. *Nat. Mater.* **12**, 139–144 (2013).
10. W. A. Phillips, Tunneling states in amorphous solids. *J. Low Temp. Phys.* **7**, 351–360 (1972).
11. S. Rau, C. Enss, S. Hunklinger, P. Neu, A. Würger, Acoustic properties of oxide glasses at low temperatures. *Phys. Rev. B* **52**, 7179–7194 (1995).
12. T. Pérez-Castañeda, C. Rodríguez-Tinoco, J. Rodríguez-Viejo, M. A. Ramos, Suppression of tunneling two-level systems in ultrastable glasses of indomethacin. *Proc. Natl. Acad. Sci. U.S.A.* **111**, 11275–11280 (2014).
13. D. R. Queen, X. Liu, J. Karel, T. H. Metcalf, F. Hellman, Excess specific heat in evaporated amorphous silicon. *Phys. Rev. Lett.* **110**, 135901 (2013).

14. D. R. Queen, X. Liu, J. Karel, H. C. Jacks, T. H. Metcalf, F. Hellman, Two-level systems in evaporated amorphous silicon. *J. Non Cryst. Solids* **426**, 19–24 (2015).
15. G. Vajente, R. Birney, A. Ananyeva, S. Angelova, R. Asselin, B. Baloukas, R. Bassiri, G. Billingsley, M. M. Fejer, D. Gibson, L. J. Godbout, E. Gustafson, A. Heptonstall, J. Hough, S. MacFoy, A. Markosyan, I. W. Martin, L. Martinu, P. G. Murray, S. Penn, S. Roorda, S. Rowan, F. Schiettekatte, R. Shink, C. Torrie, D. Vine, S. Reid, R. X. Adhikari, Effect of elevated substrate temperature deposition on the mechanical losses in tantala thin film coatings. *Class. Quantum Gravity* **35**, 075001 (2018).
16. LIGO Scientific Collaboration, Instrument Science White Paper 2020 (2020); https://dcc.ligo.org/LIGO-T2000407/public.
17. K. S. Gilroy, W. A. Phillips, An asymmetric double-well potential model for structural relaxation processes in amorphous materials. *Philos. Mag. B* **43**, 735–746 (1981).
18. R. Hamdan, J. P. Trinastic, H. P. Cheng, Molecular dynamics study of the mechanical loss in amorphous pure and doped silica. *J. Chem. Phys.* **141**, 054501 (2014).
19. Y. Levin, Internal thermal noise in the LIGO test masses: A direct approach. *Phys. Rev. D* **57**, 659–663 (1998).
20. J. Miller, L. Barsotti, S. Vitale, P. Fritschel, M. Evans, D. Sigg, Prospects for doubling the range of Advanced LIGO. *Phys. Rev. D* **91**, 062005 (2015).
21. G. Vajente, E. K. Gustafson, D. H. Reitze, Precision interferometry for gravitational wave detection: Current status and future trends. *Adv. Atom. Mol. Opt. Phys.* **68**, 75–148 (2019).
22. M. Granata, A. Amato, G. Cagnoli, M. Coulon, J. Degallaix, D. Forest, L. Mereni, C. Michel, L. Pinard, B. Sassolas, J. Teillon, Progress in the measurement and reduction of thermal noise in optical coatings for gravitational-wave detectors. *Appl. Optics* **59**, A229–A235 (2020).
23. R. Birney, J. Steinlechner, Z. Tornasi, S. MacFoy, D. Vine, A. S. Bell, D. Gibson, J. Hough, S. Rowan, P. Sortais, S. Sproules, S. Tait, I. W. Martin, S. Reid, Amorphous silicon with extremely low absorption: Beating thermal noise in gravitational astronomy. *Phys. Rev. Lett.* **121**, 191101 (2018).
24. C. R. Miranda, A. Antonelli, Transitions between disordered phases in supercooled liquid silicon. *J. Chem. Phys.* **120**, 11672–11677 (2004).
25. R. Brüning, T. Crowell, A method to determine the kinetics of a supercooled liquid by temperature scanning measurements applied to (Li, Na)acetate and GeO_2. *J. Non Cryst. Solids* **248**, 183–193 (1999).
26. R. Brüning, On the glass transition in vitreous silica by differential thermal analysis measurements. *J. Non Cryst. Solids* **330**, 13–22 (2003).
27. S. R. Elliott, Medium-range structural order in covalent amorphous solids. *Nature* **354**, 445–452 (1991).
28. M. Micoulaut, J. C. Phillips, Rings and rigidity transitions in network glasses. *Phys. Rev. B* **67**, 104204 (2003).
29. A. E. Geissberger, F. L. Galeener, Raman studies of vitreous SiO_2 versus fictive temperature. *Phys. Rev. B* **28**, 3266–3271 (1983).
30. S. Kohara, K. Suzuya, Intermediate-range order in vitreous SiO_2 and GeO_2. *J. Phys. Condens. Matter* **17**, S77–S86 (2005).
31. R. Shi, H. Tanaka, Distinct signature of local tetrahedral ordering in the scattering function of covalent liquids and glasses. *Sci. Adv.* **5**, eaav3194 (2019).
32. D. J. Durben, G. H. Wolf, Raman spectroscopic study of the pressure-induced coordination change in GeO_2 glass. *Phys. Rev. B* **43**, 2355–2363 (1991).
33. M. Micoulaut, L. Cormier, G. S. Henderson, The structure of amorphous, crystalline and liquid GeO_2. *J. Phys. Condens. Matter* **18**, R753–R784 (2006).
34. G. S. Henderson, D. R. Neuville, B. Cochain, L. Cormier, The structure of GeO_2–SiO_2 glasses and melts: A Raman spectroscopy study. *J. Non Cryst. Solids* **355**, 468–474 (2009).
35. H. Hosono, Y. Ikuta, T. Kinoshita, K. Kajihara, M. Hirano, Physical disorder and optical properties in the vacuum ultraviolet region of Amorphous SiO_2. *Phys. Rev. Lett.* **87**, 175501 (2001).
36. W. Song, X. Li, B. Wang, N. M. Anoop Krishnan, S. Goyal, M. M. Smedskjaer, J. C. Mauro, C. G. Hoover, M. Bauchy, Atomic picture of structural relaxation in silicate glasses. *Appl. Phys. Lett.* **114**, 233703 (2019).
37. N. Kaiser, Review of the fundamentals of thin-film growth. *Appl. Optics* **41**, 3053–3060 (2002).
38. L. Berthier, P. Charbonneau, E. Flenner, F. Zamponi, Origin of ultrastability in vapor-deposited glasses. *Phys. Rev. Lett.* **119**, 188002 (2017).
39. Z. Wang, T. Du, N. M. Anoop Krishnan, M. M. Smedskjaer, M. Bauchy, On the equivalence of vapor-deposited and melt-quenched glasses. *J. Chem. Phys.* **152**, 164504 (2020).
40. M. J. Hart, R. Bassiri, K. B. Borisenko, M. Véron, E. F. Rauch, I. W. Martin, S. Rowan, M. M. Fejer, I. MacLaren, Medium range structural order in amorphous tantala spatially resolved with changes to atomic structure by thermal annealing. *J. Non Cryst. Solids* **438**, 10–17 (2016).
41. A. Amato, S. Terreni, M. Granata, C. Michel, B. Sassolas, L. Pinard, M. Canepa, G. Cagnoli, Observation of a correlation between internal friction and Urbach energy in amorphous oxides thin films. *Sci. Rep.* **10**, 1670 (2020).
42. M. Granata, E. Coillet, V. Martinez, V. Dolique, A. Amato, M. Canepa, J. Margueritat, C. Martinet, A. Mermet, C. Michel, L. Pinard, B. Sassolas, G. Cagnoli, Correlated evolution of structure and mechanical loss of a sputtered silica film. *Phys. Rev. Mater.* **2**, 053607 (2018).
43. K. Prasai, J. Jiang, A. Mishkin, B. Shyam, S. Angelova, R. Birney, D. A. Drabold, M. Fazio, E. K. Gustafson, G. Harry, S. Hoback, J. Hough, C. Lévesque, I. MacLaren, A. Markosyan, I. W. Martin, C. S. Menoni, P. G. Murray, S. Penn, S. Reid, R. Robie, S. Rowan, F. Schiettekatte, R. Shink, A. Turner, G. Vajente, H.-P. Cheng, M. M. Fejer, A. Mehta, R. Bassiri, High precision detection of change in intermediate range order of amorphous zirconia-doped tantala thin films due to annealing. *Phys. Rev. Lett.* **123**, 045501 (2019).
44. J. Jiang, A. Mishkin, K. Prasai, R. Zhang, M. Yazback, R. Bassiri, M. M. Fejer, H.-P. Cheng, Analysis of two-level systems and mechanical loss in amorphous ZrO_2-doped Ta_2O_5 by non-cage-breaking and cage-breaking transitions. *J. Chem. Phys.* **154**, 174502 (2021).
45. K. G. West, J. Lu, J. Yu, D. Kirkwood, W. Chen, Y. Pei, J. Claassen, S. Wolf, Growth and characterization of vanadium dioxide thin films prepared by reactive-biased target ion beam deposition. *J. Vac. Sci. Technol. A* **26**, 133–139 (2008).
46. L. Yang, M. Fazio, G. Vajente, A. Ananyeva, G. Billingsley, A. Markosyan, R. Bassiri, M. M. Fejer, C. S. Menoni, Structural evolution that affects the room-temperature internal friction of binary oxide nanolaminates: Implications for ultrastable optical cavities. *ACS Appl. Nano Mater.* **3**, 12308–12313 (2020).
47. L. Giacomazzi, P. Umari, A. Pasquarello, Medium-range structural properties of vitreous germania obtained through first-principles analysis of vibrational spectra. *Phys. Rev. Lett.* **95**, 075505 (2005).
48. G. Vajente, A. Ananyeva, G. Billingsley, E. Gustafson, A. Heptonstall, E. Sanchez, C. Torrie, A high throughput instrument to measure mechanical losses in thin film coatings. *Rev. Sci. Instrum.* **88**, 073901 (2017).
49. E. Cesarini, M. Lorenzini, E. Campagna, F. Martelli, F. Piergiovanni, F. Vetrano, G. Losurdo, G. Cagnoli, A "gentle" nodal suspension for measurements of the acoustic attenuation in materials. *Rev. Sci. Instrum.* **80**, 053904 (2009).
50. M. Mayer, SIMNRA User's Guide (Report IPP 9/113, Max-Planck-Institut für Plasmaphysik, 1997).

Acknowledgments: The Raman scattering was performed at the Raman Microspectroscopy Laboratory in the Department of Geological Science at the University of Colorado-Boulder. **Funding:** This study was supported by the National Science Foundation (NSF) LIGO program through grant nos. 1710957 (L.Y. and C.S.M.) and 1708010 (M.F. and C.S.M.), NSF awards PHY-1707866 and PHY-1708175 (A.M., R.B., and M.M.F.), GBMF grant no. 6793 (A.M., K.P., R.B., and M.M.F.), FRQNT through the Regroupement québécois sur les matériaux de pointe (RQMP), and Natural Sciences and Engineering Research Council of Canada (M.C. and F.S.).
Author contributions: L.Y., M.F., and C.S.M. conceived the experiment. L.Y. and M.F. performed the thin-film deposition and material spectroscopy analysis. G.V., A.A., and G.B. performed the room temperature internal friction measurements. A.M., R.B., K.P., and M.M.F. contributed to the XRD measurements. M.C. and F.S. contributed to the RBS measurements. All authors contributed to the preparation of the manuscript. **Competing interests:** The authors declare that they have no competing interests. **Data and materials availability:** All data needed to evaluate the conclusions in the paper are present in the paper and/or the Supplementary Materials.

Submitted 2 March 2021
Accepted 21 July 2021
Published 10 September 2021
10.1126/sciadv.abh1117

Citation: L. Yang, G. Vajente, M. Fazio, A. Ananyeva, G. Billingsley, A. Markosyan, R. Bassiri, K. Prasai, M. M. Fejer, M. Chicoine, F. Schiettekatte, C. S. Menoni, Enhanced medium-range order in vapor-deposited germania glasses at elevated temperatures. *Sci. Adv.* **7**, eabh1117 (2021).